Materials & Biomaterials Science
Researche and Engineering

Mater. Biomater. Sci. 01 (2018) 001–005

View Journal | View Issue

ORIGINAL PAPER

The effects of bath temperature on the Zinc Oxide properties prepared by electrochemical deposition

A. Henni [a*], A. Karar [b]

[a] Lab. Dynamic Interactions and Reactivity of Systems, Kasdi Merbah University, Ouargla 30000, Algeria.
[b] Laboratoire d'Energétique et d'Electrochimie du solide, Université Ferhat Abbas-Sétif 1, Sétif 19000 Algeria.

ARTICLE INFO

Article history:
Received: 15 January 2018
Revised: 13 February 2018
Accepted: 04 Mars 2018
Published online: 11 Mars 2018

Keywords:
Electrochemical deposition
ZnO
Nanorods
Thin films
Bath temperature

ABSTRACT

In this work, Zinc oxide (ZnO) nanostructures were electrodeposited onto ITO from chloride baths at different temperatures. The electrochemical study showed that the temperature had an important effect on the current density. From the Mott-Schottky measurements, the flat-band potential and the donor density for the ZnO thin film are determined. Also, the Mott–Schottky measurements demonstrate an n-type semiconductor character for samples. Scanning electron microscopy (SEM) show arrays of vertically aligned ZnO nanorods (NRs) with good homogeneity. X-ray diffraction spectra demonstrate that films crystalline with the Würtzite structure with preferential (002) crystallographic orientation having c-axis perpendicular to the substrate. The high optical properties of the ZnO NRs with a low density of deep defects was checked by UV-Vis transmittance analyses.

Introduction

II-VI group inorganic nanoparticles such as ZnS, SnO_2, TiO_2, CdS, CdSe, ZnO, and ZnSe are well-known and have been intensively studied. ZnO is an interesting semiconductor with adirect wide bandgap (3.3 eV) and presents an excellent thermal stability, high transparency, pyroelectric and piezoelectric [1–7] properties. For these reasons, ZnO is considered as a good candidate for optical devices in the near UV region [8], and for the short wavelength-emitting devices such as light emitting diodes [2]. ZnO can be prepared by various deposition techniques such as magnetron sputtering [9], chemical vapour deposition [10], pulsed laser deposition [11], spray pyrolysis [12] or thermal evaporation [13]. Among all approaches, electrodeposition technique has been emerging as a competitive technique for the fabrication of metallic oxide semiconductor nanostructures with different shape and sizes [14–17]. Electrodeposition method has several advantages compared to other techniques: easy control of the morphology and thickness the of the film, simplicity, low equipment cost and possibility of making large-area thin films [18, 19]. For the electrodeposition of ZnO, the majority of the published works used nitrate ions or molecular oxygen [17–22] as precursors. However, few studies have been presented using hydrogen peroxide as a precursor [23].

* **Corresponding author:** Abdellah Henni
henni.abdellah@gmail.com

In this work, we report on the influence of deposition temperature on the properties of ZnO nanostructures obtained with electrochemical deposition.

Experimental

Zinc oxide thin films were prepared by electrochemical deposition (ECD) onto indium doped tin oxide (ITO, 25Ω/sq) glass coated substrates. The ITO substrates were ultrasound cleaned sequentially with acetone, ethanol and distilled water. The electrochemical deposition of ZnO was carried out in a three-electrode cell that consists a pt electrode as counter-electrode, a saturated calomel electrode as reference (SCE). The electrodeposition of ZnO nanostructures and cyclic voltammetry measurements were carried out using, a computer-controlled potentiostat/galvanostat (Autolab PGSTAT 302N) using the NOVA software. The initial solution is composed of 0.1 M KCl, 5 mM $ZnCl_2$ and 5 mM H_2O_2 [14]. The pH of solution is fixed at 6.0. Electrodeposition was performed, in a potentiostatic mode at -1.0 V vs. SCE for 40 min, at different temperatures (ranging from 40 to 70 °C).
The morphology of the product was examined by scanning electron microscopy (SEM) at medium and high magnification, respectively. The crystal structure of the sample was characterized by X-ray diffraction (XRD) using the copper K□ line under an accelerating voltage of 40 kV. The UV-Vis transmittance spectra were recorded with a Shimadzu UV-1800 spectrophotometer. The ZnO film/electrolyte capacitance measurements were performed in the same electrochemical cell with the same device as used for ZnO electrodeposition.

Results and discussion

Fig. 1 shows the cyclic voltammetric scans performed at different electrolytes (only KCl, KCl with H_2O_2 or $ZnCl_2$, KCl with H_2O_2 and $ZnCl_2$). The cyclic voltammetric measurements are performed to identify the oxidation-reduction processes potentially undergone by the system.

For the electrolyte without H_2O_2 (Fig. 1b) an oxidation peak appears when scanning back to 0.9 V vs SCE, which is due to the dissolution of zinc metal formed during forward scan.

$$Zn \longrightarrow Zn^{+2} + 2e^- \quad (1)$$

However. In the case of H_2O_2, during forward scan (Fig. 1c), a cathodic current observed relating to the following reaction [24]:

$$H_2O_2 + 2e^- \longrightarrow 2OH^- \quad (2)$$

In the presence of H_2O_2 with $ZnCl_2$ (Fig. 1d), the voltammograms shows no phenomenon other than the reduction of H_2O_2, where the amount of OH^- generated makes reaction (2) predominant. Consequently, the Zn anodic oxidation peak doesn't appear. Then, the zinc ions react with the hydroxide groups on the substrate surface to form the zinc hydroxide. Finally, Zn(OH)2 dehydrates spontaneously following:

$$Zn^{2+} + 2OH^- \longrightarrow Zn(OH)_2 \quad (3)$$

$$Zn(OH)_2 \longrightarrow ZnO + H_2O \quad (4)$$

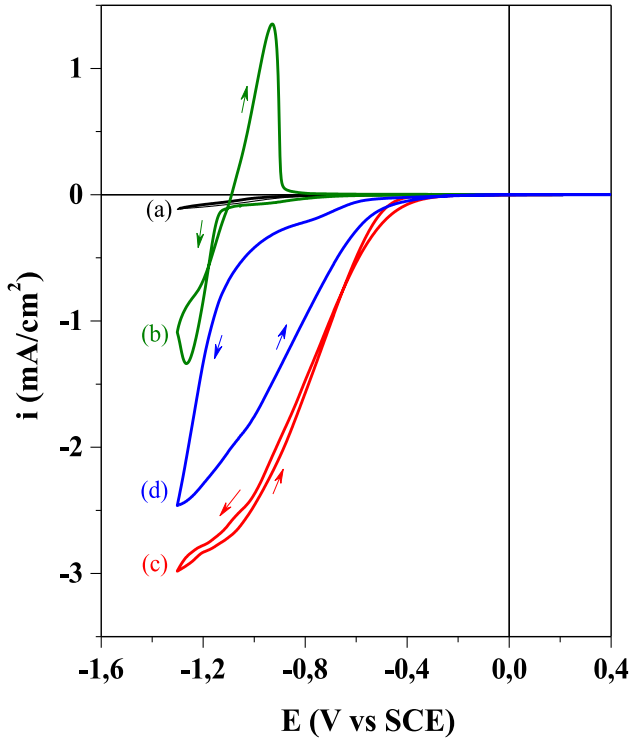

Fig. 1. Cyclic voltammetry curves recorded on ITO in aqueous solutions containing different chemical species: (a) 0.1 M KCl, (b) 0.1 M KCl + 5 mM $ZnCl_2$, (c) 0.1 M KCl + 5 mM H_2O_2 and (d) 0.1 M KCl + 5 mM H_2O_2 + 5 mM $ZnCl_2$.

In order to verify the influence of temperature on the electrochemical behavior of the electrodes in the electrodeposition bath, the cyclic voltammetry was performed.

Fig. 2 shows the voltammograms obtained at different temperatures. It is clear that the intensity of the cathode current increases with the temperature of the electrolytic bath. Indeed, in the range from 40 and 70°C, the intensity varies from –0.79 to –1.87 mA/cm², respectively. A change in the kinetics at the electrode can be accompanied by dehydration and depend on the deposition temperature.

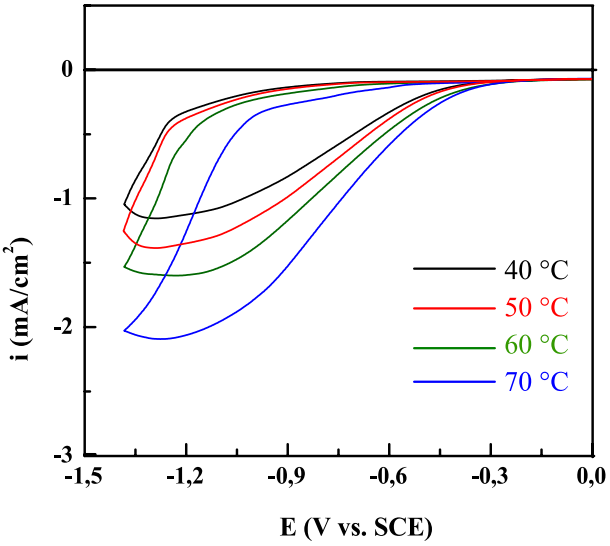

Fig. 2. Cathodic scan of 0.1 M KCl, 5mM H_2O_2 and 5mM and $ZnCl_2$ aqueous solution on a ITO electrode at different bath temperatures.

Fig. 3a shows the current transient recorded at –1.0 V vs. SCE upon ZnO deposition on ITO substrate at different temperatures. The curves confirm that the ECD ZnO are good electrical conductors, because the current density collected at the electrode is kept at about –1.4,–2.2,–2.5 and –2.9 mA.cm^{-2} after 1500 s of growth for pure ZnO (40, 50, 60 and 70°C) baths, respectively. The curves confirm the improved electrocatalytic properties of ZnO with the temperature.

The formation of ZnO nuclei on ITO begins after a very sharp increase and decline of cathodic current density early on the current transient curves of Fig. 1b. Very high cathodic current is initially required to charge an electrical double layer prior to the cathodic reduction of ZnO species. Further nucleation of ZnO or the growth of existing ZnO nuclei continues independently along with a moderate increase of cathodic current density until the highest value of cathodic current density, imax is reached except its initial surge for charging the electrical double layer. Current density decreases gradually since and stabilizes following the Cottrell equation. Maximum current (i_{max}) and time (t_{max}) values are affected the bath temperature.

Fig. 4 shows the X-ray diffraction spectra of ZnO nanostructured films grown at different bath temperatures. The films exhibit good crystallinity and all the peaks are indexed to the Würtzite hexagonal ZnO lattice (JCPDS no. 36-1451). The peaks marked with an asterisk (*) are assigned to ITO substrates, and no additional peaks corresponding to Zn or other impurities were present. The XRD patterns for all samples of ZnO show only one intense diffraction peak that located at ~34.44° which can be attributed to (002) plan, suggesting that ZnO crystallites are highly oriented with the c-axis being perpendicular to the substrate. Also, these patterns showed that the structure of the deposits was sensitive to the

bath temperature. From the XRD patterns the crystallinity of ZnO was improved by increasing deposition temperature and as consequence intensities of (002) peak also increase.

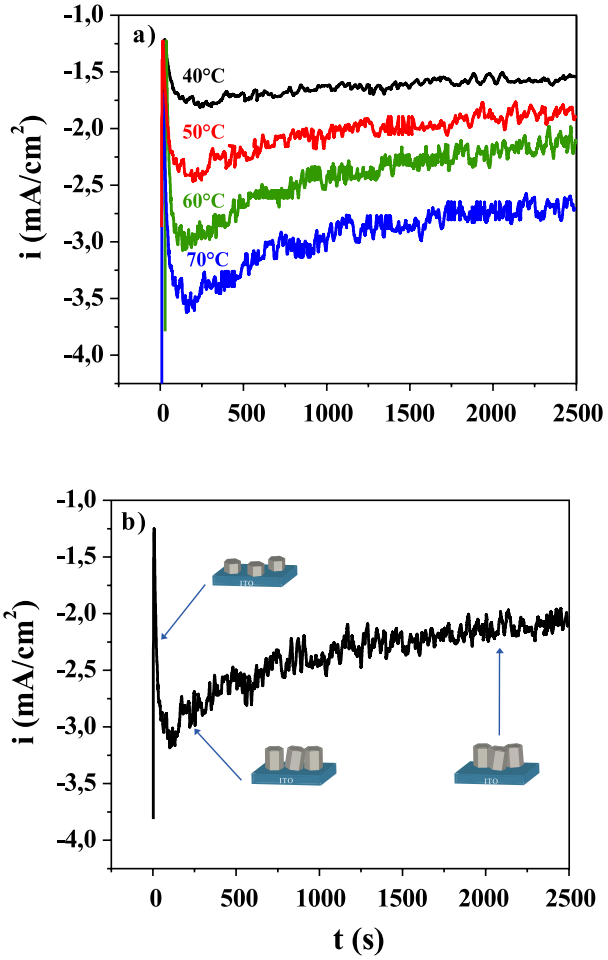

Fig. 3. Growth curves at constant applied potential of –1.0 V vs. SCE for ZnO on ITO at different bath temperatures.

Mott–Schottky measurements were used to determine both doping density and flat band potential at semiconductor/liquid contacts. Mott–Schottky plot of the space charge capacitance is presented for ZnO layers obtained at 70°C according to the following relationship [27]:

$$\frac{1}{C_{SC}^2} = \left(\frac{2}{qA^2 N_D \varepsilon \varepsilon_0}\right)\left(E - E_{fb} - \frac{kT}{q}\right) \quad (5)$$

In this equation, C^{-2}_{SC} represents the space charge capacitance, ε is the dielectric constant of ZnO, ε_0 is the permittivity of free space, N_D is the carrier concentration, E_{fb} is the flat band potential, k is Boltzmann's constant, T is the absolute temperature and q is the elementary electron charge.

According to the Mott–Schottky plot (Fig. 3b), a linear relationship of C^{-2}_{SC} vs. E was observed. The potential at which the line intersects the potential axis gives the flat band potential (E_{fb}) and the slope yields the carrier concentration (N_D) of the sample. The positive slopes of the straight line indicate the n-type conductivity of the ZnO thin film. Thus from Fig. 5a, a E_{fb} = 0.12 V was obtained and N_D = 1.5 × 1018 cm^{-3}. These values are typically those of no doping nanostructured ZnO [28].

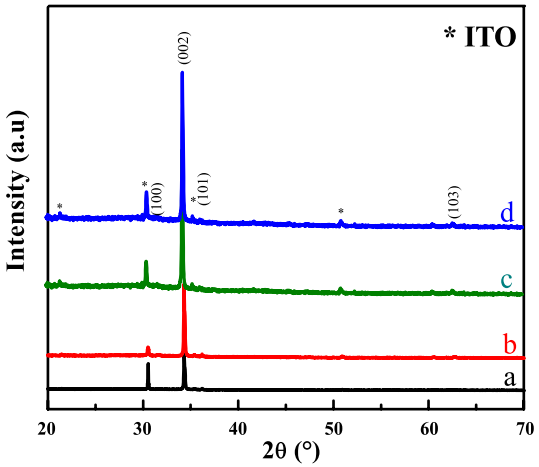

Fig. 4. XRD patterns of ZnO nanostructures deposited at various temperature : (a) 40, (b) 50, (c) 60 and (d) 70°C. XRD peaks of ITO substrate are marked by *.

Morphology of the obtained films at 70°C concentrations is presented in inset of Fig. 5b. Homogeneous ZnO nanorods have been obtained over the entire ITO substrate, which is very interesting for the realization of dye-sensitized solar cell (DSSC) [25, 26]. The nanorods act as a direct pathway for the electron transfer from the excited dye to the front contact, which favours the charge collection in the cell. The nanorods of ZnO films are hexagonal in shape with a smooth top surface, that a diameter varying in the range 115–185 nm.

The crystallites present both a lateral and a vertical growth. If the hydroxides ions generated at the electrode surface are in excess in the solution, the zinc ions present in the vicinity of the electrode are consumed rapidly and the local pH increases progressively. In first time the crystallites grow in the lateral and the vertical directions. Then, the lateral growth is then completely quenched. However, the rod growth is not fully stopped and the crystallites continue to growth but only in the c-direction (see Fig.6).

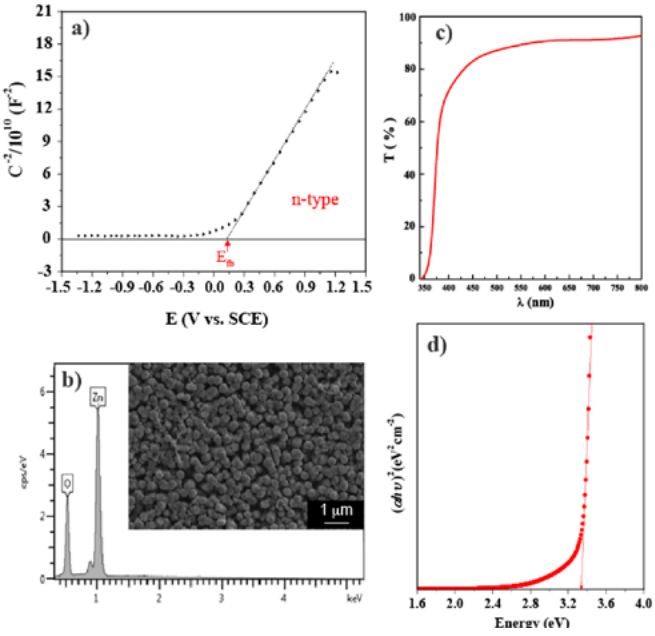

Fig. 5. a) Mott-Schottky plots recorded at 0.2 kHz, b) EDS microanalysis and SEM image, c) Transmittance spectra and d) $(\alpha h\upsilon)^2$ vs. energy dependence of a ZnO layer deposited on ITO at 70°C.

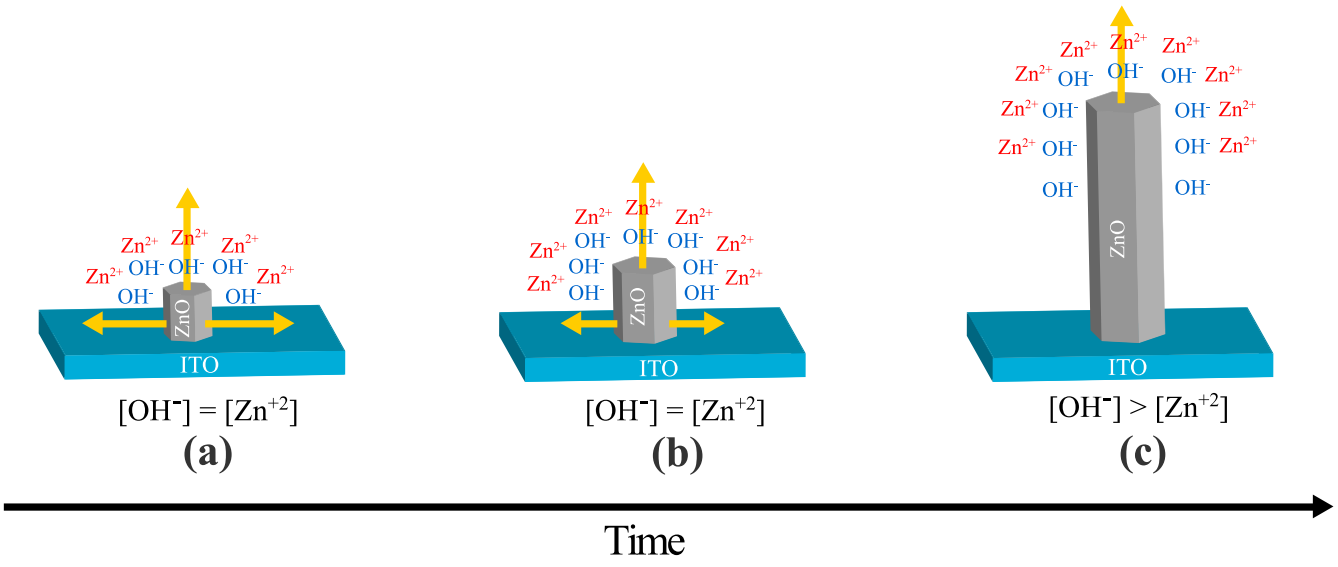

Fig. 6. Illustration of OH^- and Zn^{2+} species repartition during the ZnO nanorods growth.

The optical transmission spectra recorded in the range of 300 to 750 nm of the ZnO nanostructures deposited at 70°C are shown in Fig. 5c. We observe that the transmittance is high (~90 %). The energy band gap (E_g) for ZnO was evaluated by using the Tauc plot [29]. The value of the energy band gap of ZnO layers (Fig. 5d) is determined from the intercept of the straight-line portion at the horizontal axis when $\alpha h\upsilon = 0$, these value of E_g is 3.3 eV.

Conclusion

We have studied the effects of bath temperature on the electrodeposition of nanostructures from aqueous chloride medium. ZnO nanorods array films with good transparency, and homogeneity were successfully electrodeposited onto ITO. The optimal temperature for the growth of ZnO nanorods was established. XRD characterizations show that the films are crystallized in the Würtzite hexagonal structure with a very high crystallite orientation along the c-axis; a (002) orientation was obtained at 70°C. The SEM micrographs confirms this result, where nanorods hexagonal shapes perpendicular to the substrate surface were obtained under these conditions. The Mott-Schottky plot shows that the films are n-type semiconductors. A high apparent donor density was calculated for samples elaborated. The band gap energy values of the obtained ZnO is 3.3 eV.

References

1. S. Sepulveda-Guzman, B. Reeja-Jayan, E. de la Rosa, A. Torres-Castro, V. Gonzalez-Gonzalez, M. Jose-Yacaman, Mater. Chem. Phys. 115 (2009) 172–178.
2. O. Lupan, V.M. Guérin, I.M. Tiginyanu, V.V. Ursaki, L. Chowc, H. Heinrich, T. Pauporté, J. Photochem. Photobiol. A 211 (2010) 65–73.
3. S. O'Brien, M.G. Nolan, M. Çopuroglu, J.A. Hamilton, I. Povey, L. Pereira, R. Martins, E. Fortunato, M. Pemble, Thin Solid Films 518 (2010) 4515–4519.
4. Y. Yang, W. Guo, Ken C. Pradel, G. Zhu, Y. Zhou, Y. Zhang, Y. Hu, L. Lin, Z.L. Wang, Nano Letters 12 (2012) 2833 1493–2838.
5. D. Pradhan, K.T. Leung, Langmuir 24 (2008) 9707–9716.
6. D. Chu, T. Hamada, K. Kato,Y .Masuda, Physical Status Solidi A 206 (2009) 718–723.
7. Y.N. Chang, M. Zhang, L. Xia, J. Zhang, G. Xing, Materials 5 (2012) 2850–2871.
8. L. Luo, Y.F. Zhang, S.S. Mao, L.W. Lin, Sensor. Actuator A-Phys. 127(2006) 201–206.
9. T. Minami, T. Yamamoto, T. Miyata, Thin Solid Films 366 (2000) 63–68.
10. B.M. Ateav, A.M. Bagamadova, V.V. Mamedov, A.K. Omaev, Mater. Sci. Eng. B 65 (1999) 159–163.
11. X.W. Sun, H.S. Kwok, J. Appl. Phys. 86 (1999) 408–411.
12. A. El Hichou, M. Addou, J. Ebothé, M. Troyon, J. Lumin. 113 (2005) 183–190.
13. K. M. K. Srivatsa, D. Chhikara, M. S. Kumar, J. Mater. Sci. Technol. 27 (2011) 701–706
14. A. Henni, A. Merrouche. L. Telli, A. Azizi, R. Nechache, Sci. Semicond. Process. 31 (2015) 380–385.
15. A. Henni, A. Merrouche. L. Telli, A. Karar, FI. Ezema, H. Haffar, J. Solid State Electrochem. 20(8) (2015) 2135–2142.
16. A. Henni, A. Merrouche. L. Telli, A. Karar, J. Electroanal. Chem. 763 (2016) 149–154.
17. M.R. Khelladi, L. Mentar, A. Beniaiche, L. Makhloufi, A. Azizi, J. Mater. Sci.: Mater. Electron. 24 (2013) 153–159.
18. M. Izaki, T. Omi, Appl. Phys. Lett. 68 (1996) 2439–2440.
19. A. Goux, T. Pauporte, J. Chivot, D. Lincot, Electrochim. Acta 50 (2005) 2239–2248.
20. DK. Singh, R. Pandya, Singh, Opt. Mater. 35 (2013) 1493–1497.
21. M. Izaki, T. Omi, J. Electrochem. Soc. 143 (1996) L53–L55.
22. Z.H. Gu, T.Z. Fahidy, J. Electrochem. Soc. 146 (1999) 1561493–159.
23. D. Ramirez, D. Silva, H. Gomez, G. Riveros, R.E. Marotti, E.A. Dalchiele, Sol. Energy Mater. Sol. Cells 91 (2007) 1458–1461.
24. T. Pauporte, D. Lincot, J. Electroanal. Chem. 517 (2001) 54–62.
25. L. Qi, H. Yu, Z. Lei, Q. Wang, Q. Ouyang, C. Li, Y. Chen, Appl. Phys. A 111 (2013) 279–284.

26. M.C. Kao, H.Z. Chen, S.L. Young, Appl. Phys. A 98 (2010) 595–599.
27. S. R. Morrison, Electrochemistry at Semiconductor and Oxidized Metal Electrodes, Plenum, New York, 1980, p. 127.
28. D. Pradhan, S.K. Mohapatra, S. Tymen, M. Misra, K.T. Leung, Mater. Express 1 (2011) 59–67.
29. J. Tauc, R. Grigorovici, A. Vancu, Phys. Status Solidi 15 (1966) 627–637.

Conflicts of interest

Authors declare no conflict of interests.

Notes

The authors declare no competing financial interest.

Materials & Biomaterials Science

How to cite this article

A. Henni, A. Karar. The effects of bath temperature on the Zinc Oxide properties prepared by electrochemical deposition. Mat. Biomater. Sci. 01 (2018) 001-005.